Models for Nonheme Iron Intermediates: Structural Basis for Tuning the Spin States of Fe(TPA) Complexes

Yan Zang,[†] Jinheung Kim,[†] Yanhong Dong,[†] Elizabeth C. Wilkinson,[†] Evan H. Appelman,[‡] and Lawrence Que, Jr.*,[†]

Contribution from the Department of Chemistry and Center for Metals in Biocatalysis, University of Minnesota, Minneapolis, Minnesota 55455, and Chemistry Division, Argonne National Laboratory, Argonne, Illinois 60439

Received November 6, 1996[⊗]

Abstract: Our efforts to model the oxygen activation chemistry of nonheme iron enzymes have yielded transient intermediates with novel properties. These properties can be dramatically affected by the introduction of a 6-methyl substituent on the pendant pyridines of the tetradentate ligand TPA (TPA = tris(2-pyridylmethyl)amine). A series of Fe(TPA) complexes has thus been synthesized and characterized to provide the structural basis for these dramatic effects. The following complexes have been obtained: $[Fe(L)(CH_3CN)_2](ClO_4)_2$ (**1**, L = TPA; **2**, L = 6-MeTPA; **3**, L = 6-Me_2TPA; **4**, L = 6-Me_3TPA) and $[Fe(L)(acac)](ClO_4)_2$ (**5,** L = TPA; **6**, L = 5-Me_3TPA; **7**, L = 6-MeTPA). As indicated by ^{1}H NMR and/or EPR, **1**, **5**, and **6** with no 6-methyl substituent are low spin, while complexes **2**, **3**, **4**, and **7** with at least one 6-methyl substituent are all high spin, with higher redox potentials than their low-spin counterparts. The ligands with 6-methyl substituents thus favor a metal center with a larger ionic radius, i.e., Fe^{II} over Fe^{III} and high spin over low spin. Careful scrutiny of the crystal structures of **1**, **4**, **6**, and **7** reveals that one hydrogen of the 6-methyl group is only 2.7 Å away from the metal center in the high-spin complexes. Its presence thus prevents the pyridine nitrogen from forming an Fe−N bond shorter than 2.1 Å as required for an iron center to adopt a low-spin configuration. This steric effect of the 6-methyl substituent serves as a simple but very useful ligand design tool to tune the electronic properties of the metastable alkylperoxoiron(III) species derived from the reactions of **1**−**4** with *tert*-butyl hydroperoxide. These intermediates serve as models for low-spin and high-spin peroxoiron(III) species in the reaction cycles of the antitumor drug bleomycin and lipoxygenase, respectively. Similar principles apply in the design of nonheme diiron(II) complexes that reversibly bind dioxygen and of high-valent bis(μ-oxo)diiron complexes that model the high-valent intermediates in the redox cycles of nonheme diiron enzymes such as methane monooxygenase and ribonucleotide reductase.

Introduction

The tetradentate tripodal ligand TPA (tris(2-pyridylmethyl)-amine)[1] and its derivatives play an important and prominent role in our efforts to synthesize functional models of mononuclear and dinuclear nonheme iron oxygen activating enzymes[2,3] such as the catechol dioxygenases,[4] α-keto acid-dependent enzymes,[5] lipoxygenase,[6] ribonucleotide reductase,[7] and methane monooxygenase.[8] To date, Fe(TPA) complexes have been found to react quantitatively with O_2 to afford oxidative cleavage of 3,5-di-*tert*-butylcatechol[9] (mimicking the intradiol cleaving catechol dioxygenases) and oxidative decarboxylation of benzoylformate[10] (mimicking the α-keto acid-dependent enzymes). We have also trapped transient nonheme iron−peroxo species at low temperature from the reactions of peroxides with Fe(TPA) precursors.[11,12] Both low-spin and high-spin alkylperoxoiron(III) complexes can be obtained depending on whether TPA or 6-Me_3TPA is used in the precursor complex. The TPA species has a low-spin iron(III) center[11] like that found in "activated bleomycin",[13] while the 6-Me_3TPA species has a high-spin iron(III) center[12] like that associated with the purple form of soybean lipoxygenase.[6] Using these ligands, we also obtained $[Fe^{III}Fe^{IV}(\mu\text{-}O)_2L_2]^{3+}$, the first examples of complexes with a high-valent bis(μ-oxo)diiron diamond core,[14,15] a new structural motif that we propose for the oxidizing intermediates in the reaction of O_2 with nonheme diiron enzymes.[16] The properties of the TPA derivative indicate that it is a valence-delocalized complex consisting of double exchange-coupled low-spin Fe^{III} and Fe^{IV} centers, while those of the 6-MeTPA derivative show that it is a valence-localized

[†] University of Minnesota.

[‡] Argonne National Laboratory.

[⊗] Abstract published in *Advance ACS Abstracts,* April 15, 1997.

(1) Abbreviations: acac = 2,4-pentanedione (acetylacetone); BF = benzoylformate; bpy = bipyridine; BPA = bis(2-pyridylmethyl)amine; bpca = *N*-(2-pyridinylcarbonyl)-2-pyridinecarboximidate monoanion; HPTP = 1,3-bis[*N*,*N*-bis(2-pyridylmethyl)amino]-2-hydroxypropane; NTB = *N*,*N*,*N*-tris(2-benzimidazolylmethyl)amine; phen = 1,10-phenanthroline; salen = *N*,*N*′-ethylenebis(salicylidenamine) dianion; 5-Me_3TPA = tris[(5-methyl-2-pyridyl)methyl]amine; 6-MeTPA = bis(2-pyridylmethyl)[(6-methyl-2-pyridyl)methyl]amine; 6-Me_2TPA = bis[(6-methyl-2-pyridyl)methyl](2-pyridylmethyl)amine; 6-Me_3TPA = tris(6-methyl-2-pyridylmethyl)amine; TPA = tris[(2-pyridyl)methyl]amine; tpy = 2,2′:6′,2″-terpyridine.

(2) Que, L., Jr.; Ho, R. Y. N. *Chem. Rev.* **1996**, *96*, 2607−2624.

(3) Wallar, B. J.; Lipscomb, J. D. *Chem. Rev.* **1996**, *96*, 2625−2657.

(4) Lipscomb, J. D.; Orville, A. M. *Metal Ions Biol. Syst.* **1992**, *28*, 243−298.

(5) Abbott, M. T.; Udenfriend, S. In *Molecular Mechanisms of Oxygen Activation*; Hayaishi, O., Ed.; Academic Press: New York, 1974; pp 167−214.

(6) Nelson, M. J.; Seitz, S. In *Active Oxygen in Biochemistry*.; Valentine, J. S., Foote, C. S., Greenberg, A., Liebman, J. F., Eds.; Blackie Academic and Professional, Chapman and Hall: Glasgow, U.K., 1995; pp 276−312.

(7) Stubbe, J. *Adv. Enzymol.* **1989**, *63*, 349−419.

(8) Lipscomb, J. D. *Annu. Rev. Microbiol.* **1994**, *48*, 371−399.

(9) Jang, H. G.; Cox, D. D.; Que, L., Jr. *J. Am. Chem. Soc.* **1991**, *13*, 9200−9204.

(10) Chiou, Y.-M.; Que, L., Jr. *J. Am. Chem. Soc.* **1995**, *117*, 3999−4013.

(11) Kim, J.; Larka, E.; Wilkinson, E. C.; Que, L., Jr. *Angew. Chem., Int. Ed. Engl.* **1995**, *34*, 2048−2051.

(12) Zang, Y.; Elgren, T. E.; Dong, Y.; Que, L., Jr. *J. Am. Chem. Soc.* **1993**, *115*, 811−813.

(13) Sam, J. W.; Tang, X.-J.; Peisach, J. *J. Am. Chem. Soc.* **1994**, *116*, 5250−5256.

(14) Dong, Y.; Fujii, H.; Hendrich, M. P.; Leising, R. A.; Pan, G.; Randall, C. R.; Wilkinson, E. C.; Zang, Y.; Que, L., Jr.; Fox, B. G.; Kauffmann, K.; Münck, E. *J. Am. Chem. Soc.* **1995**, *117*, 2778−2792.

(15) Dong, Y.; Que, L., Jr.; Kauffmann, K.; Münck, E. *J. Am. Chem. Soc.* **1995**, *117*, 11377−11378.

S0002-7863(96)03852-8 CCC: $14.00

complex consisting of antiferromagnetically coupled high-spin Fe^{III} and Fe^{IV} centers. The properties of these complexes relate them to transient species observed in the oxygen activation cycles of methane monooxygenase[17−19] and ribonucleotide reductase.[20−22]

These TPA-based ligands exhibit a versatility that allows us to alter the spin state of the iron center and dramatically affect its spectroscopic properties by simply introducing a methyl substituent on the pyridine rings of TPA. Here we report the syntheses, structures, and properties of a series of iron(II) and iron(III) complexes of TPA and its methyl-substituted derivatives to provide the structural basis for the effects of introducing 6-methyl groups on the pyridine rings of TPA. These results are interpreted in the context of the properties of metastable peroxo and oxo species that have been generated as models for intermediates of nonheme iron enzymes.

Experimental Section

Syntheses. TPA·3ClO_4, 5-Me_3TPA, and 6-Me_3TPA were synthesized according to literature methods.[12,14,23,24] Commercially available chemicals were purchased and used without further purification. Elemental analyses were performed at MHW Laboratories (Phoenix, AZ). *Caution: Perchlorate salts are potentially explosive and should be handled with care*.

Bis[(6-methyl-2-pyridyl)methyl](2-pyridylmethyl)amine (6-Me_2-TPA). An aqueous NaOH solution (1 M, 5 mL) was added dropwise to a solution of (2-pyridylmethyl)amine (0.01 mol) and 2-(chloromethyl)-6-methylpyridine hydrochloride (0.02 mol) in 15 mL of water at 0 °C with stirring. The reaction mixture was then stirred for 24 h at room temperature and then extracted with $CHCl_3$. The extracts were then washed with water to remove residual NaCl, and dried over Na_2SO_4. Removal of the solvent yielded a brown solid (80% yield). ^{1}H NMR ($CDCl_3$): δ (ppm) 8.6 (1H, α-py), 7.9, 7.8, and 7.6 (6H, β-py), 7.3 (3H, γ-py), 4.5 ($2CH_2$), 4.3 (CH_2), 2.8 ($2CH_3$).

Bis(2-pyridylmethyl)[(6-methyl-2-pyridyl)methyl]amine (6-MeTPA). An aqueous NaOH solution (1 M, 3 mL) was added dropwise to a solution of bis(2-pyridylmethyl)amine (0.01 mol) and 2-(chloromethyl)-6-methylpyridine hydrochloride (0.01 mol) in 15 mL of water at 0 °C with stirring. The reaction mixture was then stirred for 24 h at room temperature and then extracted with $CHCl_3$. The extracts were then washed with water to remove residual NaCl, and dried over Na_2SO_4. Removal of the solvent yielded a dark yellow solid (70% yield). ^{1}H NMR ($CDCl_3$): δ (ppm) 8.8 (2H, α-py), 8.2, 7.8 (6H, β-py), 7.7 (3H, γ-py), 4.2 (CH_2), 4.1 ($2CH_2$), 2.7 (CH_3).

The syntheses of the Fe^{II} complexes were all carried out under Ar by Schlenk line techniques following a common procedure. Equimolar amounts of ligand and $Fe(ClO_4)_2$·$6H_2O$ were dissolved in acetonitrile, and the complex was precipitated by adding diethyl ether to this clear solution. Recrystallization from CH_3CN/ether afforded pure complexes that gave satisfactory elemental analyses.

[Fe(TPA)(CH_3CN)$_2$](ClO_4)$_2$ (1). Anal. Calcd for $C_{22}H_{24}Cl_2FeN_6O_8$: C, 43.13; H, 3.86; N, 13.40. Found: C, 42.87; H, 3.86; N, 12.91.

[Fe(6-MeTPA)(CH_3CN)$_2$](ClO_4)$_2$ (2). Anal. Calcd for $C_{23}H_{26}Cl_2FeN_6O_8$: C, 43.07; H, 4.06; N, 13.11. Found: C, 43.24; H, 4.31; N, 12.96.

[Fe(6-Me_2TPA)(CH_3CN)$_2$](ClO_4)$_2$·$4H_2O$ (3). Anal. Calcd for $C_{24}H_{36}Cl_2FeN_6O_{12}$: C, 39.62; H, 4.99; N, 11.55. Found: C, 39.82; H, 4.76; N, 11.29.

[Fe(6-Me_3TPA)(CH_3CN)$_2$](ClO_4)$_2$ (4). Anal. Calcd for $C_{25}H_{30}Cl_2FeN_6O_8$: C, 43.86; H, 4.52; N, 12.56. Found: C, 43.45; H, 4.81; N, 12.71.

The three iron(III) acac complexes were synthesized using the following procedure. Equimolar amounts of $Fe(ClO_4)_3$·$6H_2O$ and ligand were dissolved in methanol. To this solution was added 1 equiv each of Hacac and Et_3N in methanol, turning the solution deep purple in color. After the solution stood overnight in the refrigerator, dark crystalline needles were obtained.

[Fe(TPA)(acac)](ClO_4)$_2$ (5). Anal. Calcd for $C_{23}H_{25}Cl_2FeN_4O_{10}$: C, 42.88; H, 3.91; N, 8.70. Found: C, 42.69; H, 4.05; N, 8.63.

[Fe(5-Me_3TPA)(acac)](ClO_4)$_2$·H_2O (6). Anal. Calcd for $C_{26}H_{33}Cl_2FeN_4O_{11}$: C, 44.33; H, 4.72; N, 7.95. Found: C, 44.49; H, 4.81; N, 7.97.

[Fe(6-MeTPA)(acac)](ClO_4)$_2$ (7). Anal. Calcd for $C_{24}H_{27}Cl_2FeN_4O_{10}$: C, 43.79; H, 4.13; N, 8.51. Found: C, 43.72; H, 4.48; N, 8.33.

^{t}BuOOH-d_9 was synthesized by adding an ethereal solution of ^{t}BuMgCl-d_9 via a syringe pump to a flask containing diethyl ether at −78 °C while simultaneously bubbling dry O_2 gas through the diethyl ether, and purified according to the method of Walling and Buckler.[25] The Grignard reagent was prepared according to standard methods[26] from ^{t}BuCl-d_9, which was prepared from ^{t}BuOH-d_9 and concentrated HCl.

^{t}BuO^{18}OH was synthesized by the reaction of ^{t}BuOH with $H^{18}OF$.[27] The latter was prepared as a stabilized 0.6 M solution in acetonitrile by passing molecular fluorine (20% in Ar) through 11 mL of a chilled 8% v/v solution of ^{18}O-enriched water (96 atom % ^{18}O, Monsanto Research Corp.) in CH_3CN.[28−30] The resulting solution was shaken with silica gel to remove excess HF and residual water. It was then mixed with 2 mL of ^{t}BuOH and allowed to stand for several hours at room temperature to ensure complete reaction. Residual HF was removed by stirring overnight with calcium carbonate (Merck SupraPur) and filtering. Concentration by evaporation at room temperature (with some loss) yielded 3 mL of a ca. 0.7 M solution of labeled ^{t}BuOOH.

Preparation of Intermediates. All intermediates were prepared according to the general procedure outlined below. A 2−5 mM acetonitrile solution of the iron(II)−acetonitrile complex was cooled to −40 °C, and then 5 equiv of ^{t}BuOOH was added to this cold solution. The deep blue or purple (depending on ligand) intermediate which forms immediately upon addition of ^{t}BuOOH was used for spectroscopic measurements.

Physical Methods. ^{1}H NMR spectra were recorded on a Varian Unity 300 or 500 spectrometer at ambient temperature. Chemical shifts (ppm) were referenced to the residual protic solvent peaks. EPR spectra were obtained at liquid helium temperatures on a Varian E-109 spectrometer equipped with an Oxford ESR-10 cryostat. Low-temperature visible spectra were recorded on a Hewlett-Packard 8452 diode array spectrophotometer using an immersion dewar equipped with quartz windows and filled with methanol chilled with liquid N_2.

Electrochemical studies were carried out with a BAS 100 electrochemical analyzer (Bioanalytical Systems, Inc., West Lafayette, IN) in acetonitrile using 0.1 M tetraethylammonium perchlorate as the supporting electrolyte. Cyclic voltammograms (CV) were obtained by using a three-component system consisting of a platinum disk working electrode, a platinum wire auxiliary electrode, and a silver wire as the reference electrode. Potentials were corrected to the NHE standard by measuring the ferrocenium/ferrocene couple under the same conditions (+400 mV vs NHE).

(16) Que, L., Jr.; Dong, Y. *Acc. Chem. Res.* **1996**, *29*, 190−196.
(17) Lee, S.-K.; Fox, B. G.; Froland, W. A.; Lipscomb, J. D.; Münck, E. *J. Am. Chem. Soc.* **1993**, *115*, 6450−6451.
(18) Lee, S.-K.; Nesheim, J. C.; Lipscomb, J. D. *J. Biol. Chem.* **1993**, *268*, 21569−21577.
(19) Liu, K. E.; Valentine, A. M.; Wang, D.; Huynh, B. H.; Edmondson, D. E.; Salifoglou, A.; Lippard, S. J. *J. Am. Chem. Soc.* **1995**, *117*, 10174−10185.
(20) Bollinger, J. M., Jr.; Edmondson, D. E.; Huynh, B. H.; Filley, J.; Norton, J.; Stubbe, J. *Science (Washington, D.C.)* **1991**, *253*, 292−298.
(21) Ravi, N.; Bollinger, J. M., Jr.; Huynh, B. H.; Edmondson, D. E.; Stubbe, J. *J. Am. Chem. Soc.* **1994**, *116*, 8007−8014.
(22) Sturgeon, B. E.; Burdi, D.; Chen, S.; Huynh, B. H.; Edmondson, D. E.; Stubbe, J.; Hoffman, B. M. *J. Am. Chem. Soc.* **1996**, *118*, 7551−7557.
(23) Anderegg, G.; Wenk, F. *Helv. Chim. Acta* **1967**, *50*, 2330−2332.
(24) Gafford, B. G.; Holwerda, R. A. *Inorg. Chem.* **1989**, *28*, 60−71.
(25) Walling, C.; Buckler, S. A. *J. Am. Chem. Soc.* **1955**, *77*, 6032−6038.
(26) Furniss, B. S.; Hannaford, A. J.; Smith, P. W. G.; Tatchell, A. R. *Vogel's Textbook of Practical Organic Chemistry*; Longman Scientific & Technical: New York, 1989; pp 534−535.
(27) Appelman, E. H.; Thompson, R. C.; Engelkemeir, A. G. *Inorg. Chem.* **1979**, *18*, 909−911.
(28) Rozen, S.; Brand, M. *Angew. Chem., Int. Ed. Engl.* **1986**, *25*, 554−555.
(29) Rozen, S.; Brand, M.; Kol, M. *J. Am. Chem. Soc.* **1989**, *111*, 8325−8326.
(30) Appelman, E. H.; Dunkelberg, O.; Kol, M. *J. Fluorine Chem.* **1992**, *56*, 199−213.

Table 1. Crystallographic Data

	1	**4**	**6**	**7**
formula	$C_{70}H_{64}B_2FeN_6$	$C_{73}H_{80}B_2FeN_6$	$C_{26}H_{31}Cl_2FeN_4O_{10}$	$C_{24}H_{27}Cl_2FeN_4O_{10}$
formula weight, amu	1066.79	1108.87	686.31	658.25
space group	*Pbca*	$P2_12_12_1$	$P2_1/n$ (no. 14)	$P2_1/c$ (no. 14)
a, Å	20.030(8)	14.398(5)	12.448(3)	8.7805(1)
b, Å	17.00(1)	17.172(7)	17.704(4)	9.0849 (3)
c, Å	33.22(3)	24.503(8)	13.515(4)	35.1580 (9)
β, deg	90	90	96.77(3)	96.500 (1)
V, Å^3	11312(10)	6058(6)	2958(2)	2789.70 (12)
Z	8	4	4	4
D(calc), g cm^{-3}	1.265	1.227	1.541	1.567
temperature, K	172	172	172	172
λ, Å	0.710 69	0.710 73	0.710 69	0.710 73
μ, cm^{-1}	3.12	3.93	7.5	0.795
R^a	0.094	0.089	0.073	0.0939[b]
R_w	0.091	0.083	0.072	0.1957[c]

[a] $R = (\sum||F_o| - |F_c||)/(\sum|F_o|)$; $R_w = \{(\sum w|F_o - F_c|^2)/(\sum w(F_o)^2)\}^{1/2}$. [b] $R_1 = \sum||F_o| - |F_c||/\sum|F_o|$. [c] $wR_2 = (\sum[w(F_o^2 - F_c^2)^2]/\sum[wF_o^4])^{1/2}$, where $w = q/\sigma^2(F_o^2) + (aP)^2 + bP$.

Resonance Raman spectra were recorded on a Spex 1403 double monochromator interfaced with a Spex DM3000 data system using a Spectra Physics 2030-15 argon ion laser to pump a 375B CW dye laser (rhodamine 6G). Spectra were obtained at 77 K using a back-scattering geometry with $\lambda_{ex} = 599.5$ nm. Samples were frozen onto a gold-plated copper cold finger in thermal contact with a dewar containing liquid nitrogen.[31] Raman shifts of spectral features were referenced to ν_1 of frozen acetonitrile (922 cm^{-1}) which was in turn referenced to the emission spectrum of a low-pressure Hg lamp.

Electrospray ionization mass spectral data were collected using a Sciex API III mass spectrometer (Sciex, Thornhill, Ontario, Canada). Cooled CH_3CN (dry ice on the syringe) was introduced by a syringe infusion pump (model 22, Harvard Apparatus, South Natick, MA) through a 76 μm internal diameter fused silica capillary line for about 20 min, and then the cooled sample solution was introduced. The instrument was scanned in 0.2 Da steps and a 5−10 ms dwell time per step; signal averaging was used to enhance the signal-to-noise ratio.

Crystallographic Studies. Crystals of the complexes were mounted onto a glass fiber and cooled to −100 °C. For the Fe^{II} complexes crystals were coated with a viscous hydrocarbon in an anaerobic box before being mounted to prevent oxidation. Data collection and analysis were conducted at the X-ray Crystallographic Laboratory of the Chemistry Department of the University of Minnesota.

For crystals **1**, **4**, and **6**, data were collected on an Enraf-Nonius CAD-4 diffractometer with graphite monochromated Mo Kα (λ = 0.710 69 Å) radiation. Cell constants and orientation matrices for data collection were obtained from a least squares refinement using the setting angles of 25 carefully centered reflections. The intensities of three representative reflections were measured every 50 min of X-ray exposure time throughout the data collection to ascertain crystal integrity, and no decay in intensity was observed. All data were corrected for empirical absorption and Lorentz and polarization effects. Pertinent crystallographic data and experimental conditions are summarized in Table 1. The structures were solved by direct methods. All non-hydrogen atoms were refined either anisotropically or isotropically, and hydrogen atoms were placed in calculated positions (d_{C-H} = 0.95 Å) and assigned thermal parameters that were 20% greater than the B_{equiv} value of the atom to which they were bonded and not refined. Refinement was carried out with full matrix least squares on *F* with scattering factors from ref 32 and included anomalous dispersion terms. Selected bond lengths and bond angles are listed in Tables 2 and 3.

For complex **7**, data were collected on a Siemens SMART system. An initial set of cell constants was calculated from reflections harvested from three sets of 20−30 frames. These initial sets of frames are oriented such that orthogonal wedges of reciprocal space are surveyed. This produces orientation matrices determined from 50−300 reflections. Final cell constants were calculated from a set that did not exceed a number equal to 8192 of strong reflections from the actual data collection. Pertinent crystallographic data and experimental conditions are summarized in Table 1. The structure was solved by direct methods. All non-hydrogen atoms were refined anisotropically, and hydrogen atoms were placed in ideal positions and refined as riding atoms with individual (or group if appropriate) isotropic displacement parameters. Selected bond lengths and bond angles are listed in Table 3.

Table 2. Selected Bond Lengths and Bond Angles for $[Fe(TPA)(CH_3CN)_2]^{2+}$ (**1**) and $[Fe(6\text{-}Me_3TPA)(CH_3CN)_2]^{2+}$ (**4**)

Bond Lengths (Å)

	1		**4**	
Fe1−N_{amine}	(N1)	1.99(1)	(N1A)	2.15(1)
Fe1−N_{py}	(N11)	1.97(1)	(N11A)	2.25(1)
	(N21)	1.92(1)	(N31A)	2.18(1)
	(N31)	1.95(1)	(N21A)	2.24(1)
Fe1−$N_{acetonitrile}$	(N41)	1.92(1)	(N41A)	2.17(1)
	(N51)	1.93(1)	(N51A)	2.17(1)

Bond Angles (deg)

1			**4**
N1−Fe1−N11	84.7(5)	N1A−Fe1−N11A	76.9(5)
N1−Fe1−N21	85.6(6)	N1A−Fe1−N31A	81.8(5)
N1−Fe1−N31	82.8(5)	N1A−Fe1−N21A	76.2(5)
N1−Fe1−N41	178.6(6)	N1A−Fe1−N41A	170.1(5)
N1−Fe1−N51	93.8(5)	N1A−Fe1−N51A	87.7(5)
N21−Fe1−N41	93.7(6)	N31A−Fe1−N41A	107.8(5)
N41−Fe1−N51	86.8(6)	N41A−Fe1−N51A	82.5(5)

Table 3. Selected Bond Lengths and Bond Angles for $[Fe(5\text{-}Me_3TPA)(acac)]^{2+}$ (**6**) and $[Fe(6\text{-}MeTPA)(acac)]^{2+}$ (**7**)

Bond Lengths (Å)

	6		**7**	
Fe−N_{amine}	(N1)	1.968(5)	(N1)	2.143(6)
Fe−N_{py}	(N2)	1.980(5)	(N4)	2.161(7)
	(N3)	1.926(5)	(N2)	2.072(6)
	(N4)	1.958(5)	(N3)	2.144(6)
Fe−O_{acac}	(O1)	1.902(4)	(O2)	1.951(5)
	(O2)	1.872(4)	(O1)	1.909(5)

Bond Angles (deg)

6			**7**
N1−Fe−N3	87.1(2)	N1−Fe1−N2	82.4(2)
N1−Fe−N2	84.0(2)	N1−Fe1−N4	77.8(3)
N1−Fe−N4	81.7(2)	N1−Fe−N3	76.5(3)
O1−Fe−N2	92.9(2)	O2−Fe1−N4	89.2(2)
O1−Fe−N4	90.8(2)	O2−Fe1−N3	95.0(2)
O2−Fe−N2	94.4(2)	O1−Fe1−N4	111.4(2)
O2−Fe−N4	99.8(2)	O1−Fe1−N3	94.1(2)

Results and Discussion

Our efforts to model the active sites of non-heme iron proteins have focused mainly on the tripodal TPA ligand and its 6-methyl

(31) Czernuszewicz, R. C.; Johnson, M. K. *Appl. Spectrosc.* **1983**, *37*, 297−298.

(32) Cromer, D. T.; Waber, J. T. *International Tables for X-ray Crystallography*; Kynoch Press: Birmingham, England, 1974; Vol. IV.

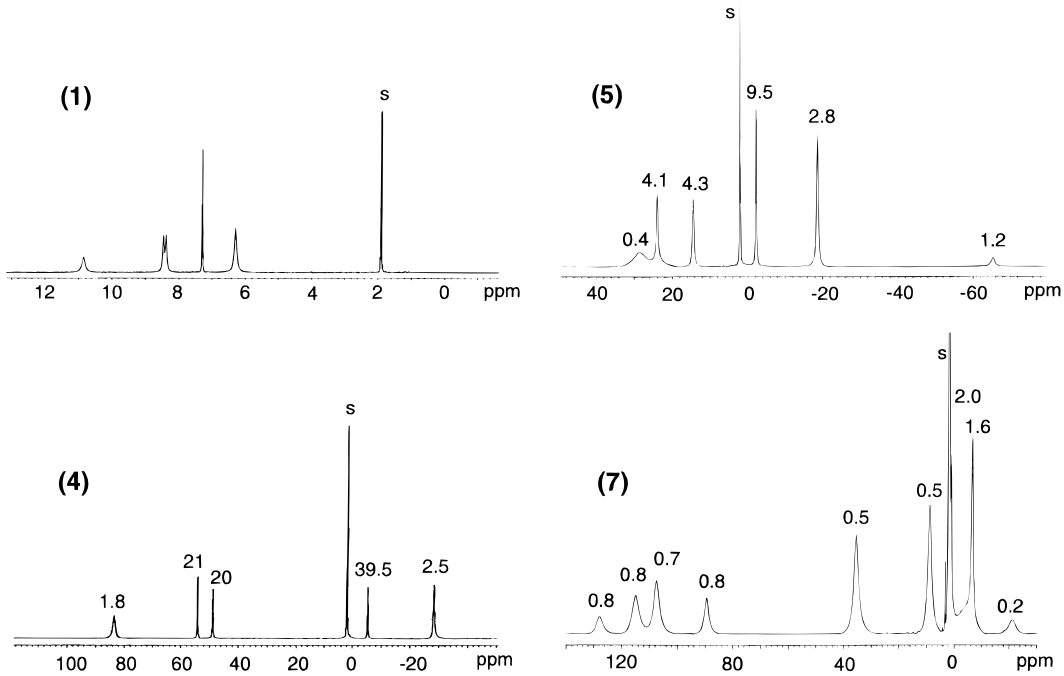

Figure 1. ^{1}H NMR spectra of complexes **1**, **4**, **5**, and **7** in CD_3CN at room temperature. T_1 values (ms) are shown on the top of the peak. Solvent peaks are labeled "s".

Table 4. ^{1}H NMR, EPR, and Electrochemical Properties of Complexes

	^{1}H NMR (ppm)								
	tripodal ligand				acac				
complex[a]	α-H (CH_3)	β,β′-H (CH_3)	γ-H	CH_2	CH_3	CH_3	CH	EPR *g* values	$E_{1/2}$ (mV)
1	10.9	8.5, 8.4	7.3	6.3					860
2	95	48, 52	−7	88					940[b]
	(−24)	51, 50	−6	82, 37					
3	106	56, 59	−11	92					940[b]
	(−25)	52, 57	−6	86, 75					
4	(−28)	49, 54	−5	83					940[b]
5	28.6	24, 14.4	−2.3	28.6	−18.5	−18.5	−65	2.57, 235, 1.71	70
6	32	16, (1.6)	−3.4	32	−17.6	−17.6	−63.4	2.57, 2.35, 1.71	20
7	c	115, 108	−6.5	c	35	9	−21	4.50, 430, 4.15	175
	(−5)	128, 89	1.2	c					

[a] **1** = $[Fe(TPA)(CH_3CN)_2](ClO_4)_2$; **2** = $[Fe(6\text{-}MeTPA)(CH_3CN)_2](ClO_4)_2$; **3** = $[Fe(6\text{-}Me_2TPA)(CH_3CN)_2](ClO_4)_2$; **4** = $[Fe(6\text{-}Me_3TPA)(CH_3CN)_2](ClO_4)_2$; **5** = $[Fe(TPA)(acac)](ClO_4)_2$; **6** = $[Fe(5\text{-}Me_3TPA)(acac)](ClO_4)_2$; **7** = $[Fe(6\text{-}MeTPA)(acac)](ClO_4)_2$. [b] Only an irreversible oxidation peak observed. [c] Too broad to be observed.

derivatives. When 6-methyl substituents on the pyridine rings are introduced, we observe significant changes in the properties of the corresponding complexes.[12,14,15] We have thus synthesized a series of Fe^{II} and Fe^{III} complexes with TPA, 6-MeTPA, 6-Me_2TPA, and 6-Me_3TPA in order to study systematically the effects of increasing 6-methyl substitution on the properties of the iron centers in these complexes and establish the basis for these dramatic effects.

Iron(II) Complexes. The synthesis of the series of iron(II) complexes $[Fe(L)(CH_3CN)_2]^{2+}$ (L = TPA, 6-MeTPA, 6-Me_2-TPA, and 6-Me_3TPA) is straightforward; crystalline products were obtained by simply mixing iron(II) perchlorate and the appropriate ligand in acetonitrile and precipitating the desired complex with ether. However, these iron(II) complexes have very different properties. The ^{1}H NMR spectrum of **1** in CD_3CN at room temperature exhibits features of a diamagnetic species, demonstrating that the Fe^{II} center in **1** is low spin (Figure 1, Table 4). Unlike the low-spin complex **1**, complex **4** has a ^{1}H NMR spectrum typical of a high-spin Fe^{II} complex with peaks paramagnetically shifted over a range of −30 to +80 ppm (Figure 1, Table 4). These peaks can be assigned by comparison to the spectra of other high-spin Fe^{II}TPA[33] and 6-Me_3TPA complexes.[10] The ^{1}H NMR spectra of **2** and **3** (Table 4) show that both are high-spin iron(II) complexes. Thus, the introduction of even one 6-methyl substituent to TPA is sufficient to change the iron(II) center from low spin to high spin in the $[Fe^{II}L(CH_3CN)_2]^{2+}$ series.

Cyclic voltammetric measurements on **1**−**4** (Table 4) show that the iron(II) oxidation state is greatly favored by these ligand environments. Complex **1** shows a quasi-reversible cyclic voltammogram with $E_{1/2}$ = 860 mV vs NHE (ΔE = 80 mV, i_{pa}/i_{pc} = 0.75), its high redox potential may be attributed to the thermodynamic stability of the low-spin Fe(II) state by analogy to $[Fe(bpy)_3]^{2+}$ and related complexes.[34] Complexes **2**−**4** are also oxidized at high potential (∼940 mV), but the oxidations are irreversible in these cases. Since these three are all high-spin complexes, factors other than spin state must disfavor the iron(III) oxidation state in these complexes.

Iron(III) Complexes. Unlike the iron(II) complexes, the synthesis of a similar series of $[Fe^{III}L(acac)]^{2+}$ complexes

(33) Zang, Y.; Que, L., Jr. *Inorg. Chem.* **1995**, *34*, 1030−1035.
(34) Fukuzumi, S.; Kochi, J. K. *J. Am. Chem. Soc.* **1982**, *104*, 7599−7609.

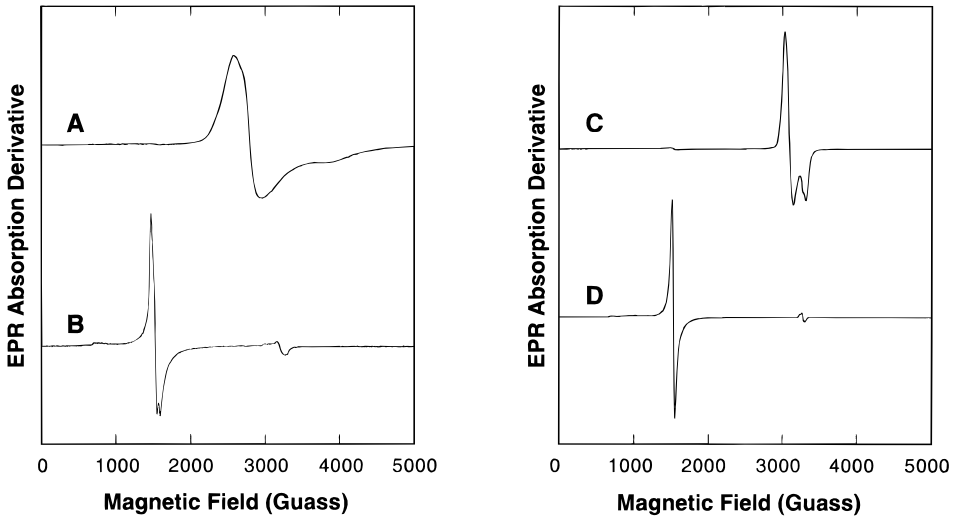

Figure 2. X-band EPR spectra recorded at 2 K. Typical EPR conditions: microwave frequency 9.23 GHz; microwave power 0.2 mW; modulation amplitude 10 G; modulation frequency 100 KHz. (a) [Fe(TPA)(acac)](ClO$_4$)$_2$ (**5**). (b) [Fe(6-MeTPA)(acac)](ClO$_4$)$_2$ (**7**). (c) [Fe(TPA)(H$_2$O)(OO^{t}Bu)](ClO$_4$)$_2$ (**1a**). (d) [Fe(6-Me$_3$TPA)(H$_2$O)(OO^{t}Bu)](ClO$_4$)$_2$ (**4a**).

presented varying degrees of difficulty. The two ligands without 6-substituents, TPA and 5-Me$_3$TPA, form stable iron(III) complexes, but the stability of the complexes decreases significantly as the number of 6-methyl substituents increases. 6-MeTPA forms an iron(III) complex that decomposes slowly in solution over a period of weeks, while attempts to synthesize [Fe(6-Me$_2$TPA)(acac)]$^{2+}$ and [Fe(6-Me$_3$TPA)(acac)]$^{2+}$ by mixing the ligand, Fe^{III}(ClO$_4$)$_3$, and Hacac have produced free ligand and Fe(acac)$_3$ instead. We tried to prepare [Fe(6-Me$_2$TPA)(acac)]$^{2+}$ and [Fe(6-Me$_3$TPA)(acac)]$^{2+}$ by oxidizing the corresponding iron(II) complexes, but only observe the yellow solutions of [FeL(acac)](ClO$_4$) (L = 6-Me$_2$TPA, 6-Me$_3$TPA) convert to the red color characteristic of Fe(acac)$_3$. These results show that the introduction of two or three 6-methyl substituents to the TPA ligand significantly destabilizes the [Fe^{III}L(acac)]$^{2+}$ complexes.

[Fe(TPA)(acac)]$^{2+}$ (**5**) (Figure 2a) and [Fe(5-Me$_3$TPA)(acac)]$^{2+}$ (**6**) show EPR signals at g = 2.57, 2.35, and 1.71, typical of low-spin Fe^{III} centers.[35] On the other hand, **7** shows EPR signals (Figure 2b) at g_1 = 4.50, g_2 = 4.30, and g_3 = 4.15, which can be ascribed to the middle Kramers doublet of an S = 5/2 system with E/D = 0.31, demonstrating that the Fe^{III} in **7** is high spin. ^{1}H NMR shifts of the iron(III) complexes are consistent with the EPR results (Table 4). [Fe(TPA)(acac)]$^{2+}$ (**5**) (Figure 1) and [Fe(5-Me$_3$TPA)(acac)]$^{2+}$ (**6**) exhibit ^{1}H NMR spectra with relatively sharp signals characteristic of low-spin Fe^{III} complexes. [Fe(6-MeTPA)(acac)]$^{2+}$ (**7**), on the other hand, exhibits a ^{1}H NMR spectrum (Figure 1, Table 4) typical of mononuclear high-spin Fe^{III} complexes with larger paramagnetic shifts and broader signals like those in [Fe(TPA)X$_2$]$^+$ (X = Cl$^-$, Br$^-$) complexes.[36] The peak assignments are listed in Table 4.

The effects of introducing a methyl group are also reflected in the redox properties of the Fe^{III}acac complexes. Complexes **5**−**7** each display a reversible redox wave with $E_{1/2}$ values at 70 mV (ΔE = 75 mV, i_{pa}/i_{pc} = 1.00), 20 mV (ΔE = 70 mV, i_{pa}/i_{pc} = 1.01), and 175 mV (ΔE = 90 mV, i_{pa}/i_{pc} = 1.01) relative to NHE, respectively. Methyl substitution on the pyridine ring of the tripodal ligand should make the pyridine more basic and lower the redox potential of the metal center as observed in the 50 mV decrease in potential on going from **5** to **6**, which has three 5-methyl substituents. However, the opposite shift is observed on going from **5** to **7**, which has one 6-methyl substituent, showing that the iron(II) oxidation state is favored in **7**. This shift is consistent with the observation that Fe^{III}acac complexes of 6-Me$_2$TPA and 6-Me$_3$TPA could not be isolated. Similar upshifts in the redox potentials of dimanganese complexes have been noted by Hodgson and co-workers upon introduction of a 6-methyl substituent.[37] Crystal structures of these iron complexes provide the rationale for this behavior.

Crystal Structures. ORTEP plots for the cations **1** and **4** are shown in Figure 3. The iron(II) center in each complex is in a distorted octahedral environment ligated by the three pyridine nitrogens and one amine nitrogen of the tripodal ligand and two acetonitrile nitrogens. Although **1** and **4** have similar coordination geometries, the Fe−N bond lengths and bond angles differ greatly between these two complexes, reflecting the difference in spin state (Table 2). For example, the Fe−N$_{amine}$ distance of 1.99(1) Å in **1** is significantly shorter than the Fe−N$_{amine}$ distance of 2.15(1) Å in **4**. Likewise, the Fe−N$_{py}$ bond distances of **1** are 0.25−0.29 Å shorter than the corresponding Fe−N$_{py}$ bonds in **4**. The average Fe−N$_{py}$ distance of 1.95 Å found in **1** is comparable to those typically found in low-spin iron(II) complexes, such as [Fe(phen)$_3$]$^{2+}$ (1.97 Å),[38] [Fe(bpy)$_3$]$^{2+}$ (1.96 Å),[39] [Fe(tpy)$_2$]$^{2+}$ (1.96 Å),[40] [Fe(BPA)$_2$]$^{2+}$ (1.97 Å),[41] and [Fe(bpca)$_2$] (1.94 Å).[42] On the other hand, the average Fe−N$_{py}$ of 2.22 Å in **4** is comparable to those found in [Fe$_2$(6-Me$_3$TPA)$_2$F$_2$]$^{2+}$ (2.24 Å),[43] [Fe(6-Me$_3$TPA)(OBz)]$^+$ (2.21 Å),[12] and [Fe(6-Me$_3$TPA)(BF)]$^+$ (2.22 Å),[10] but slightly longer than those found in high-spin Fe^{II}TPA complexes.[10,33,43,44] The bond length difference between high-spin TPA and 6-Me$_3$TPA complexes is very likely due to the steric effects of the 6-methyl substituents which prevent the pyridines from approaching the metal center too closely. Similar elonga-

(35) Burger, R. M.; Peisach, J.; Horwitz, S. B. *J. Biol. Chem.* **1981**, *256*, 11636−11644.
(36) Kojima, T.; Leising, R. A.; Yan, S.; Que, L., Jr. *J. Am. Chem. Soc.* **1993**, *115*, 11328−11335.
(37) Goodson, P. A.; Oki, A. R.; Glerup, J.; Hodgson, D. J. *J. Am. Chem. Soc.* **1990**, *112*, 6248−6254.
(38) Zalkin, A.; Templeton, D. H.; Ueki, T. *Inorg. Chem.* **1973**, *12*, 1641−1646.
(39) Posse, G. M. E.; Juri, M. A.; Aymonino, P. J.; Piro, O. E.; Negri, H. A.; Castellano, E. E. *Inorg. Chem.* **1984**, *23*, 948.
(40) Baker, A. T.; Goodwin, H. A. *Aust. J. Chem.* **1985**, *38*, 207−214.
(41) Butcher, R.; Addison, A. W. *Inorg. Chim. Acta* **1989**, *158*, 211−215.
(42) Wocadlo, S.; Massa, W.; Folgado, J. *Inorg. Chim. Acta* **1993**, *207*, 199−206.
(43) Zang, Y.; Jang, H. G.; Chiou, Y.-M.; Hendrich, M. P.; Que, L., Jr. *Inorg. Chim. Acta* **1993**, *213*, 41.
(44) Ménage, S.; Zang, Y.; Hendrich, M. P.; Que, L., Jr. *J. Am. Chem. Soc.* **1992**, *114*, 7786−7792.

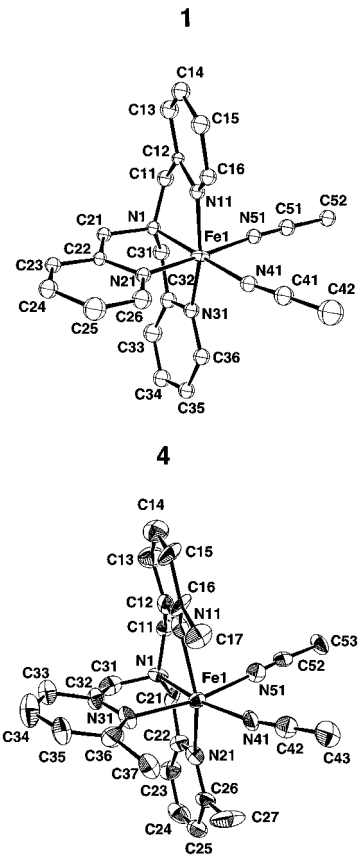

Figure 3. ORTEP plots of $[Fe(TPA)(CH_3CN)_2]^+$ (**1**) and $[Fe(6\text{-}Me_3\text{-}TPA)(CH_3CN)_2]^+$ (**4**). Ellipsoids are drawn at the 50% probability level. Hydrogen atoms are omitted for clarity.

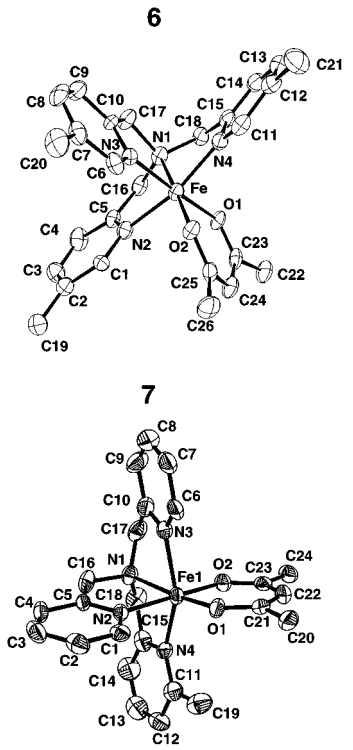

Figure 4. ORTEP plots of $[Fe(5\text{-}Me_3TPA)(acac)]^{2+}$ (**6**) and [Fe(6-MeTPA)(acac)]$^{2+}$ (**7**). Ellipsoids are drawn at the 50% probability level. Hydrogen atoms are omitted for clarity.

tion of the metal-to-nitrogen distances upon 6-methyl substitution has also been observed by Hodgson *et al.*[37] and Suzuki *et al.*[45]

The steric effects of the 6-methyl groups are also reflected by the bond angles. The coordination geometry is more distorted from an ideal octahedron in **4**. The angles that differ most significantly are ∠N21−Fe−N41 in **1** (93.7(6)°) and the corresponding ∠N31A−Fe−N41A in **4** (107.8(5)°), because the 6-methyl substituent (C27, Figure 3) pushes the acetonitrile away. This effect is also seen in ∠N1−Fe−N41 which is 178.6(6)° in **1**, very close to the ideal 180°, but only 170.1(5)° in **4**. The average ∠N1−Fe−N_{py} angle is 84.4° in **1** and is 78.3° in **4**, smaller than 90° because of the five-membered chelate ring size imposed by the tripodal ligands. Other high-spin Fe(TPA) and Fe(6-Me_3TPA) complexes also exhibit small ∠N_{amine}−Fe−N_{py} angles, averaging ca. 77°.[43,46]

ORTEP plots for the iron(III) complexes [Fe(5-Me_3TPA)-(acac)]$^{2+}$ (**6**) and [Fe(6-MeTPA)(acac)]$^{2+}$ (**7**) are shown in Figure 4. The Fe^{III} center is six-coordinate in each complex with four nitrogens from the tripodal ligand and two oxygens from the acac. The acac is chelated slightly asymmetrically to the iron with the shorter Fe−O bond *trans* to the amine nitrogen ($\Delta r_{Fe-O} = 0.03$ Å for **7** compared to $\Delta r_{Fe-O} = 0.05$ Å for [Fe-(salen)(acac)][47] and $\Delta r_{Fe-O} = 0.09$ Å for [Fe(NTB)(acac)]$^{2+}$ [48]). Like the iron(II) complexes, the bond lengths and bond angles differ significantly between **6** and **7** (Table 3). In **6**, where the 5-methyl substituents point away from the iron, there are no steric effects. The average Fe−N_{py} distance of 1.96 Å and Fe−N_{amine} of 1.968(5) Å are about 0.2 Å shorter than those of high-spin iron(III) TPA complexes.[9,46,49] The Fe−O bonds of 1.872(5) and 1.902(5) Å in **6** are also 0.1 Å shorter than those of $Fe(acac)_3$ (av 1.99 Å).[50] These results are consistent with the low-spin state of the iron in **6**. On the other hand, the introduction of a 6-methyl group on only one pyridine in **7** results in the lengthening of the average Fe−N_{py} distance to 2.125 Å, comparable to corresponding values for [Fe(TPA)-Cl_2]$^+$ (2.150 Å)[36] and other high-spin Fe^{III}(TPA) complexes. The Fe−O_{acac} bonds in **7** have also lengthened to 1.909(5) and 1.951(5) Å. The average ∠N1−Fe−N_{py} angle is 84.3° in **6** and 78.9° in **7**.

The 6-methylpyridine pendant ligand has the longest of the three Fe−N_{py} distances (2.161(7) Å), reflecting the steric effect of the 6-methyl group. It is interesting to note that the tripodal ligand does not adopt the most symmetric configuration in the structure of **7**. Such a configuration would entail having the 6-methylpyridine pendant ligand coordinate *trans* to an acac oxygen and in the plane of the acac. This arrangement would cause the 6-methyl substituent to run into an acac methyl group, but is avoided by having the 6-methylpyridine pendant occupy a position *cis* to the oxygen and perpendicular to the acac plane. Other structural features also reflect the steric effects of the 6-methyl group in **7**. The acac ligand is bent away from the pendant 6-methylpyridine to avoid the steric interactions as indicated by ∠O1−Fe−N4 (111.3°) which is much bigger than ∠O1−Fe−N3 (94°). In **6** the corresponding angles are 99.8° and 94.4°, respectively.

These structural features rationalize the relative stabilities of the $[Fe^{III}L(acac)]$ series of complexes. For 6-Me_3TPA with 6-methyl groups on all three pyridines, one of the methyl groups will run into a methyl group of the acac ligand; hence, $[Fe^{III}$(6-

(45) Hayashi, Y.; Kayatani, T.; Sugimoto, H.; Suzuki, M.; Inomata, K.; Uehara, A.; Mizutani, Y.; Kitagawa, T.; Maeda, Y. *J. Am. Chem. Soc.* **1995**, *117*, 11220−11229.
(46) Norman, R. E.; Yan, S.; Que, L., Jr.; Sanders-Loehr, J.; Backes, G.; Ling, J.; Zhang, J. H.; O'Connor, C. J. *J. Am. Chem. Soc.* **1990**, *112*, 1554−1562.
(47) Lauffer, R. B.; Heistand, R. H.; Que, L., Jr. *Inorg. Chem.* **1983**, *22*, 50.
(48) Nazikkol, C.; Wegner, R.; Bremer, J.; Krebs, B. *Z. Anorg. Allg. Chem.* **1996**, *622*, 329−336.
(49) Ménage, S.; Que, L., Jr. *New J. Chem.* **1991**, *15*, 431−438.
(50) Iball, J.; Morgan, C. H. *Acta Crystallogr.* **1967**, *33*, 239−244.

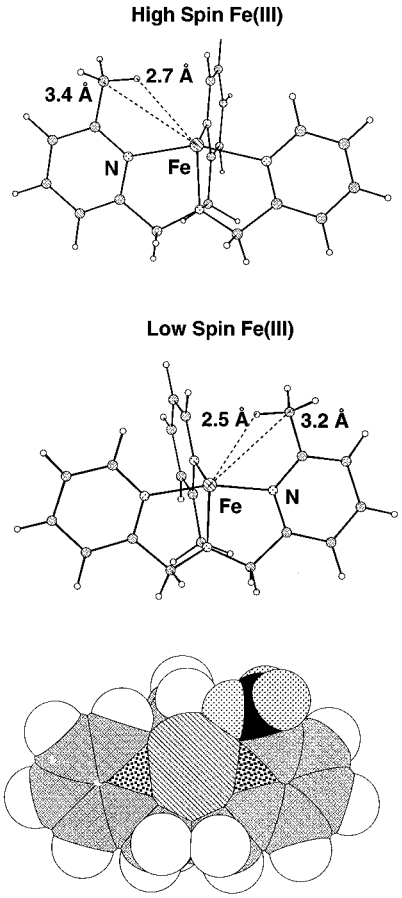

Figure 5. Steric interactions of the 6-methyl substituent with the iron atom. The top structure is from the crystal structure of **7** with the acac ligand omitted for clarity. The middle structure is generated with CSC Chem3D with Fe−N_{py} bonds of 1.95 Å. A space-filling model to illustrate the Fe−H interaction is shown on the bottom.

Me_3TPA)(acac)]$^{2+}$ is unstable. The corresponding 6-Me_2TPA complex [Fe^{III}(6-Me_2TPA)(acac)]$^{2+}$ is also unstable, even though the two 6-methylpyridines can coordinate *trans* to each other and avoid running into a methyl group of the acac; however, with *trans*-6-methyl groups on the tripodal ligand, the acac has no space to bend away from the 6-methylpyridine pendants to relieve the steric interactions and yet remain coordinated to the iron.

Careful scrutiny of space-filling models of **4** and **7** as well as [Fe_2O_2(6-Me_3TPA)$_2$]$^{2+}$ [51] and [Fe_2O(OH)(6-Me_3TPA)$_2$]$^{3+}$ [52] provides some insight into the steric effects of the 6-methyl substituent. Figure 5 depicts the interaction between the 6-methyl group and the iron center. The top structure is from the crystal structure of **7** with the acac ligand omitted for clarity. It shows that a hydrogen on the 6-methyl group is only 2.7 Å away from the iron center. Shortening the Fe−N_{py} bond by 0.2 Å as required by a low-spin iron center (middle structure in Figure 5 as generated with CSC Chem3D) would increase the unfavorable steric interactions between the 6-methyl substituent and the iron center; these interactions prevent the pyridyl nitrogen from getting any closer to the iron center than ca. 2.15 Å. Thus, the introduction of even one 6-methyl substituent affords high-spin complexes. The addition of two other 6-methyl groups gives rise to additional steric interactions that result in even longer Fe−N bonds (∼2.23 Å) as found in all structurally characterized 6-Me_3TPA complexes.[43,51]

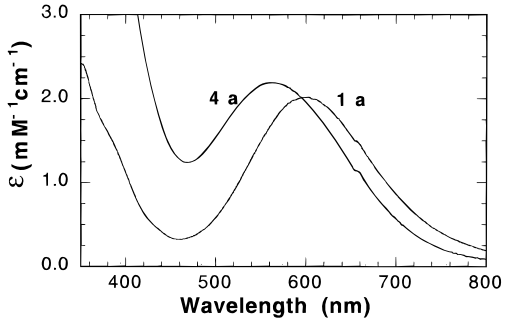

Figure 6. Absorption spectra of [Fe(TPA)(H_2O)(OO^tBu)](ClO_4)$_2$ (**1a**) and [Fe(6-Me_3TPA)(H_2O)(OO^tBu)](ClO_4)$_2$ (**4a**) in CH_3CN at −40 °C.

Applications to the Transient Intermediates. Our systematic study of complexes **1**−**7** has demonstrated that the introduction of a 6-methyl substituent on a pyridine of a TPA ligand exerts a significant effect on the spin state of the iron center, engendering dramatic changes in the properties of the iron complex and its derivatives. Due to steric interactions with the iron center, the 6-methyl-substituent prevents the pyridine ligand from approaching the iron center too closely, making the 6-methyl-substituted pyridine a much weaker ligand than its intrinsic basicity may initially suggest. Thus, the 6-methyl-substituted TPAs favor iron states with larger ionic radii, viz., high-spin over low-spin and Fe^{II} over Fe^{III}. Consequently low-spin Fe(TPA) complexes become high-spin upon the introduction of a 6-methyl substituent. The stabilization of the iron(II) state for ligands with 6-methyl substituents is reflected in the higher redox potentials of **2**−**4** and the instability of the iron(III)acac complexes of tripodal ligands with 6-methyl substituents.

The effects of a 6-methyl substituent are also reflected in the properties of transient alkylperoxoiron(TPA) species we have characterized in our efforts to understand the oxygen activation mechanisms of mononuclear nonheme iron active sites. Thus, treatment of **1** with a slight excess of ^{t}BuOOH at −40 °C in CH_3CN affords a transient blue intermediate, **1a**, with spectroscopic properties essentially identical to those of the compound derived from the reaction of [Fe_2O(TPA)$_2$(H_2O)$_2$]$^{4+}$ with excess ^{t}BuOOH.[11] Species **1a** exhibits an absorption spectrum (Figure 6) with a maximum near 600 nm ($\epsilon \approx 2200$ M^{-1} cm^{-1}) and EPR signals (Figure 2c) at $g = 2.19$, 2.14, and 1.98, which indicate that it is a low-spin iron(III) complex. Double integration reveals that the EPR signals account for all the iron, indicating that the Fe^{II} center in **1** is completely oxidized to the Fe^{III} oxidation state. Electrospray ionization mass spectral analysis shows that **1a** is an alkylperoxoiron(III) complex. The positive ion mass spectrum exhibits two intense peaks at m/z = 452 and 534, corresponding to the ions {[Fe^{III}(TPA)(OH)(OO^tBu)]}$^+$ and {[Fe^{III}(TPA)(OO^tBu)](ClO_4)}$^+$, respectively (Figure 7). Similarly, its negative ion mass spectrum shows two peaks at m/z = 650 and 732 corresponding to the ions {[Fe^{III}(TPA)(OH)(OO^tBu)](ClO_4)$_2$}$^-$ and {[Fe^{III}(TPA)(OO^t-Bu)](ClO_4)$_3$}$^-$, respectively. The formulations for these ions are all corroborated by isotope distribution patterns that match the calculated patterns. In this regard, the perchlorate counterions are particularly useful as they produce isotope patterns diagnostic of the number of anions and therefore the charge of the complex cation.[53] From the nature of the ions produced, we deduce that **1a** has the composition [Fe^{III}(TPA)(OH_2)(OO^t-Bu)]ClO_4.

Related alkylperoxo species can also be obtained by the reaction of ^{t}BuOOH with **2**−**4** in CH_3CN at −40 °C. As with

(51) Zang, Y.; Dong, Y.; Que, L., Jr.; Kauffnann, K.; Münck, E. *J. Am. Chem. Soc.* **1995**, *117*, 1169−1170.

(52) Zang, Y.; Pan, G.; Que, L., Jr.; Fox, B.; Münck, E. *J. Am. Chem. Soc* **1994**, *116*, 3653−3654.

(53) Kim, J.; Dong, Y.; Larka, E.; Que, L., Jr. *Inorg. Chem.* **1996**, *35*, 2369−2372.

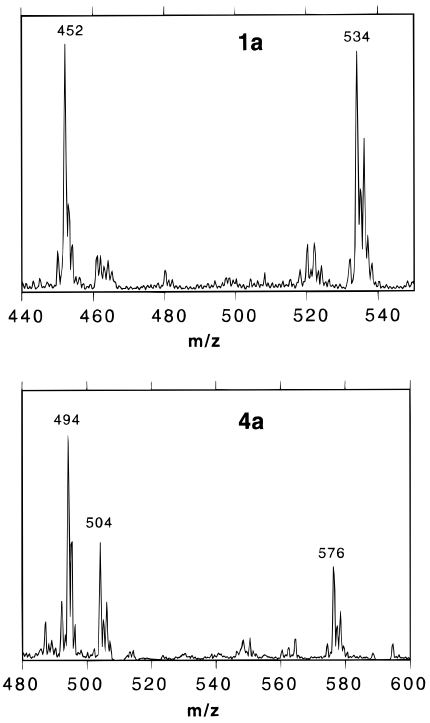

Figure 7. Positive ion electrospray ionization mass spectra of [Fe(TPA)(H_2O)(OO^tBu)](ClO_4)$_2$ (**1a**) and [Fe(6-Me_3TPA)(H_2O)(OO^tBu)](ClO_4)$_2$ (**4a**).

Table 5. Spectroscopic Properties of the Alkylperoxo Intermediates

intermediate[a]	λ_{max} (nm)	EPR *g* values	Raman shifts (cm^{-1})			
1a	600	2.19, 2.14, 1.98	490	696	796	
1a(^{t}BuO^{18}OH)			488	638, 657, 672	778	
1a(^{t}BuOOH-d_9)			450	668, 700	803	
2a	598	2.20, 2.12, 1.97	488	682	790	
		4.3	469	648	842	878
3a	552	4.3	470	647	843	881
4a	562	4.3	468	637	842	877
4a(^{t}BuO^{18}OH)			463	612	829	867
4a(^{t}BuOOH-d_9)			422	622		860
8a	514	4.3	464	648	844	880

[a] [FeL(H_2O)(OO^tBu)](ClO_4)$_2$ in CH_3CN (**1a**, L = TPA; **2a**, L = 6-MeTPA; **3a**, L = 6-Me_2TPA; **4a**, L = 6-Me_3TPA; **8a**, [Fe(6-Me_3TPA)(OBz)(OO^tBu)](ClO_4)$_2$ in CH_2Cl_2 (from ref 12).

1a, intermediates **2a**−**4a** each exhibit a strong absorption band in the region of 550−600 nm with extinction coefficients of *ca*. 2000 M^{-1} cm^{-1} (Figure 6, Table 5). The electrospray ionization mass spectra of **4a** (Figure 7) exhibit positive ions at m/z = 494 and 576 corresponding to {[Fe^{III}(6-Me_3TPA)(OH)(OO^tBu)]}$^+$ and {[Fe^{III}(6-Me_3TPA)(OO^tBu)](ClO_4)}$^+$, respectively, and negative ions at m/z = 692 and 774 which correspond to {[Fe^{III}(6-Me_3TPA)(OH)(OO^tBu)](ClO_4)$_2$}$^-$ and {[Fe^{III}(6-Me_3TPA)(OO^tBu)](ClO_4)$_3$}$^-$, respectively. The mass difference of 42 units between corresponding ions of **1a** and **4a** reflects the mass difference between TPA and 6-Me_3TPA. The electrospray ionization mass spectral data thus demonstrate that the intermediates are alkylperoxoiron(III) complexes with the formula [Fe^{III}(L)(OH_2)(OO^tBu)]ClO_4.

Unlike **1a**, the EPR spectra of intermediates **2a**−**4a** (Table 5) indicate the presence of high-spin Fe^{III} species. Intermediates **3a** and **4a** exhibit isotropic EPR signals (Figure 2d) at g = 4.3, characteristic of a high-spin iron(III) complex in a rhombic environment. Double integration of these signals reveals that all the iron centers have been converted to this EPR-active form. Interestingly, **2a** exhibits EPR signals at g = 4.3 and in the g = 2 region, indicating that **2a** is a mixture of high-spin and low-spin Fe^{III} components. Thus, as observed in the precursor complexes, the parent TPA ligand gives rise to a low-spin iron(III)−alkylperoxo species, while the 6-Me_2TPA and 6-Me_3TPA ligands afford the corresponding high-spin iron(III) species. The introduction of one 6-methyl substituent engenders an intermediate situation with both spin states accessible.

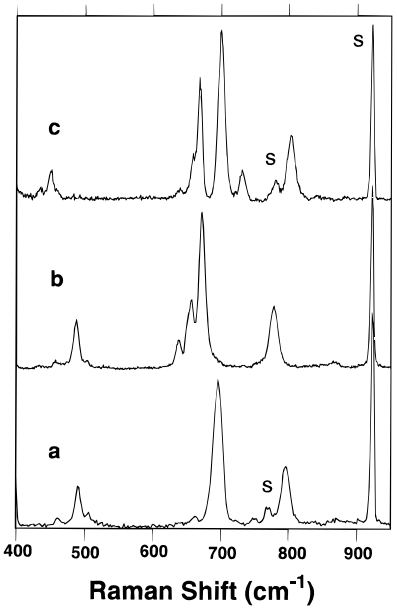

Figure 8. Resonance Raman spectra of intermediates obtained with 599 nm excitation on frozen CH_3CN solutions: (a) **1a** (from ^{t}BuOOH), (b) **1a** (from ^{t}BuO^{18}OH), (c) **1a** (from ^{t}BuOOH-d_9). Solvent bands are labeled "s".

The low-spin and the high-spin alkylperoxo intermediates each show a distinctive pattern in their resonance Raman spectra. Low-spin **1a** exhibits three peaks at 796, 696, and 490 cm^{-1} (Figure 8), identical to those observed for the intermediate derived from [$Fe_2O(TPA)_2(H_2O)_2$]$^{4+}$ and ^{t}BuOOH[11] and similar to the low-spin iron(III) species obtained from [$Fe(III)_2O(bpy)_4(H_2O)_2$]($ClO_4$)$_4$ and ^{t}BuOOH.[54] The 796 and 696 cm^{-1} peaks are sensitive to the introduction of both ^{18}O into the terminal peroxo oxygen and ^{2}H into the alkyl methyl groups, while the 490 cm^{-1} peak is only sensitive to ^{2}H substitution and shifts to 450 cm^{-1} when ^{t}BuOOH-d_9 is used. The position of the 490 cm^{-1} peak (below 500 cm^{-1}), the 40 cm^{-1} shift to lower energy upon deuteration of the *tert*-butyl group, and the insensitivity to ^{18}O substitution all argue for the assignment of this band as the C−C−C deformation of the *tert*-butyl group.[55] The shifts in the peaks at 796 and 696 cm^{-1} are less straightforward to explain. The peroxide moiety is a strong Raman scatterer, and so we expect to see an intense feature in the 800−900 cm^{-1} region resulting from the O−O stretch. The *tert*-butyl group complicates the vibrational spectrum of *tert*-butyl peroxide because the C−O linkage has a vibration of energy similar to that of the O−O linkage; therefore, these coordinates couple extensively. There can also be contributions from the carbon skeleton as suggested by a normal coordinate analysis of *tert*-butyl alcohol.[56] This analysis demonstrates that the intense, polarized vibration at 780 cm^{-1} in the Raman spectrum of liquid $(CH_3)_3COH$ involves approximately 67% C−O stretching and 33% symmetric CC_4 stretching. The sensitivity of the peaks at 796 and 696 cm^{-1} to both ^{18}O at the terminal oxygen and deuterium in the methyl groups shows that these vibrations involve motion of the alkyl group as well as the C−O and O−O

(54) Ménage, S.; Wilkinson, E. C.; Que, L., Jr.; Fontecave, M. *Angew. Chem., Int. Ed. Engl.* **1995**, *34*, 203−205.
(55) Dollish, F. R.; Fateley, W. G.; Bentley, F. F. *Characteristic Raman Frequencies of Organic Compounds*; Wiley: New York, 1974; pp 1−6.
(56) Tanaka, C. *Nippon Kagaku Zasshi* **1962**, *83*, 398−405.

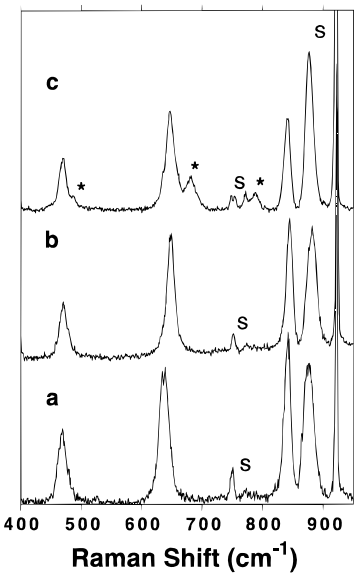

Figure 9. Resonance Raman spectra of intermediates obtained with 514.5 nm excitation on frozen CH_3CN solutions: (a) **4a** (from ^{t}BuOOH), (b) **3a** (from ^{t}BuOOH), (c) **2a** (from ^{t}BuOOH; peaks marked with an asterisk are from the low-spin isomer). Solvent bands are labeled "s".

linkages. We propose that the peak at 696 cm^{-1} is a vibration of the ^{t}BuO moiety but also involving some O−O stretching component. The peak at 796 cm^{-1} actually moves to higher energy (803 cm^{-1}) when the ^{t}BuOO$^-$ ligand is deuterated, which suggests that the symmetric CC_4 stretching component has become uncoupled from the O−O stretch. Thus, the 796 and 696 cm^{-1} peaks are assigned to be vibrations comprising O−O stretching, C−O stretching, and symmetric CC_4 stretching of the *tert*-butyl group, with greater contribution of O−O stretching to the 796 cm^{-1} peak.

The high-spin intermediate **4a** shows a different pattern of Raman shifts with peaks at 877, 842, 637, and 468 cm^{-1} (Figure 9); a similar pattern is observed for the intermediate **8a** derived from the reaction of [Fe(II)(6-Me$_3$TPA)(OBz)]$^+$ (**8**) and ^{t}BuOOH (Table 5).[12] Unlike the low-spin intermediates, all four peaks of **4a** are affected by the introduction of terminally ^{18}O-labeled ^{t}BuOOH or deuteration of the *tert*-butyl group (Table 5), indicating that the entire molecule is involved in all four vibrations. This greater complexity precludes a detailed assignment of the vibrations at present, and more detailed isotope labeling experiments are needed to fully assign these peaks.[57] Nevertheless, it is clear that **1a** and **4a** exhibit distinct Raman spectra. Furthermore, high-spin **3a** has the same Raman spectrum as that of **4a**, while **2a** exhibits the features associated with both high-spin and low-spin iron(III)−alkylperoxo complexes. Thus, the spectral distinctions correlate with spin state rather than a difference in peroxide coordination mode as earlier suggested.[12] Indeed the data accumulated thus far for this series indicate that these complexes are all terminal η^1-alkylperoxo complexes.

Intermediates **1a**−**4a** represent the first characterized nonheme alkylperoxoiron(III) complexes and serve as models for metastable biologically relevant peroxoiron(III) complexes such as "activated bleomycin" which has a low-spin iron(III) center[13,58] and the purple lipoxygenase complex which has a high-spin iron(III) center.[6] The above series exemplifies a simple ligand design strategy in which the introduction of a 6-methyl substituent on a pyridine of a TPA ligand significantly affects the electronic properties of the metal center.

There are two other examples in the literature of the effects of 6-methyl substituents on pyridine rings on the properties of transient iron intermediates. The first example involves the reversibility of dioxygen adduct formation from diiron(II) complexes of dinucleating ligands with pendant pyridines. We have shown that exposure of $[Fe^{II}_2(HPTP)(O_2CC_6H_5)]^{2+}$ to O_2 affords an irreversible O_2 adduct,[59,60] while Suzuki et al. have found that the introduction of 6-methyl substituents renders such adducts reversible.[45] For the parent complex, the diiron(III) state is strongly favored, so O_2 binding is irreversible. Introducing the 6-methyl substituents destabilizes the diiron(III) state and shifts the redox potential of the diiron center to more positive values, thereby making O_2 binding reversible.

The second striking example involves a pair of synthetic bis(μ-oxo)diiron(III,IV) complexes which serve as the only synthetic precedents for high-valent intermediates in the reactions of dioxygen with the reduced nonheme diiron enzymes such as methane monooxygenase (MMO)[17−19] and ribonucleotide reductase (RNR).[20−22] The TPA derivative has a valence-delocalized, presumably double exchange-coupled low-spin iron(III)−low-spin iron(IV) center with a novel $S = 3/2$ ground state.[14] Introducing only one 6-methyl substituent on the ligand makes the irons high spin, so the 6-MeTPA derivative[15] has a valence-localized antiferromagnetically coupled high-spin iron(III)−high-spin iron(IV) center. The TPA derivative has Mössbauer parameters that resemble MMO intermediate **Q** which is proposed to be a diiron(IV) species,[17] while the 6-MeTPA derivative has EPR properties that resemble intermediate **X** of ribonucleotide reductase.[22] These similarities form the basis for a mechanistic hypothesis in which the Fe_2O_2 diamond core serves as the common repository for the oxidizing equivalents in the redox cycles of nonheme diiron enzymes.[16]

In summary, this study provides the structural basis for using 6-methyl substituents on pyridine rings to tune the properties of an iron center and demonstrates the utility of this simple ligand design tool to obtain models for transient intermediates in the catalytic cycles of nonheme iron enzymes.

Acknowledgment. This work was supported by the National Institutes of Health (Grant GM 33162). The National Science Foundation provided funds for the purchase of the Siemens SMART system. We thank Dr. Albert Jache for assistance in the preparation of the labeled ^{t}BuOOH, which was carried out at Argonne National Laboratories under the auspices of the Office of Basic Energy Sciences, Division of Chemical Sciences, U.S. Department of Energy. We also thank Professor Doyle Britton and Dr. Victor Young, Jr., for solving the crystal structures.

Supporting Information Available: Tables listing experimental details of X-ray structure determinations, atomic coordinates, isotropic and anisotropic thermal parameters, and all bond lengths and angles for **1**, **4**, **6**, and **7** (76 pages). See any current masthead page for ordering and Internet access instructions.

JA9638521

(57) In support of this complexity, only three higher frequency vibrations of the intermediate derived from the reaction of **8** and cumene hydroperoxide are sensitive to ^{18}O-labeling. See ref 12.

(58) Burger, R. M.; Kent, T. A.; Horwitz, S. B.; Münck, E.; Peisach, J. *J. Biol. Chem.* **1983**, *258*, 1559−1564.

(59) Dong, Y.; Ménage, S.; Brennan, B. A.; Elgren, T. E.; Jang, H. G.; Pearce, L. L.; Que, L., Jr. *J. Am. Chem. Soc.* **1993**, *115*, 1851−1859.

(60) Dong, Y.; Yan, S.; Young, V. G., Jr.; Que, L., Jr. *Angew. Chem., Int. Ed. Engl.* **1996**, *35*, 618−620.